



Antivirulence Isoquinolone Mannosides: Optimization of the Biaryl Aglycone for FimH Lectin Binding Affinity and Efficacy in the Treatment of Chronic UTI

Cassie Jarvis,^[a] Zhenfu Han,^[a] Vasilios Kalas,^[b] Roger Klein,^[b] Jerome S. Pinkner,^[b] Bradley Ford,^[b] Jana Binkley,^[b] Corinne K. Cusumano,^[b] Zachary Cusumano,^[d] Laurel Mydock-McGrane,^[d] Scott J. Hultgren,^{*,[b, c]} and James W. Janetka^{*,[a, c]}

Uropathogenic *E. coli* (UPEC) employ the mannose-binding adhesin FimH to colonize the bladder epithelium during urinary tract infection (UTI). Previously reported FimH antagonists exhibit good potency and efficacy, but low bioavailability and a short half-life in vivo. In a rational design strategy, we obtained an X-ray structure of lead mannosides and then designed mannosides with improved drug-like properties. We show that cyclizing the carboxamide onto the biphenyl B-ring aglycone of biphenyl mannosides into a fused heterocyclic ring, generates new biaryl mannosides such as isoquinolone **22** (2-methyl-4-(1-oxo-1,2-dihydroisoquinolin-7-yl)phenyl α -D-mannopyranoside) with enhanced potency and in vivo efficacy resulting from increased oral bioavailability. N-Substitution of the isoquinolone aglycone with various functionalities produced a new potent subseries of FimH antagonists. All analogues of the subseries have higher FimH binding affinity than unsubstituted lead **22**, as determined by thermal shift differential scanning fluorimetry assay. Mannosides with pyridyl substitution on the isoquinolone group inhibit bacteria-mediated hemagglutination and prevent biofilm formation by UPEC with single-digit nanomolar potency, which is unprecedented for any FimH antagonists or any other antivirulence compounds reported to date.

Urinary tract infections (UTIs) represent the second most common infectious disease, imposing enormous socioeconom-

ic and healthcare burdens worldwide. UTIs predominantly afflict women, who have a lifetime risk of 50% for developing an acute infection and 20% for experiencing multiple, recurrent infections.^[1] Antibiotic resistance^[2] among uropathogenic *E. coli* (UPEC), which account for the overwhelming majority of UTIs, is a rising problem. In addition, the ability of UPEC to establish quiescent reservoirs may lead to the observed recalcitrance to antibiotic therapy, as chronic bladder reservoirs may serve as seeds for recurrent UTI and contribute to the troubling nature of this disease.^[3] Furthermore, a history of UTI significantly predisposes one to recurrent UTI.^[4] Thus, antibiotic-sparing approaches, such as antivirulence strategies^[5] that prevent UPEC colonization, represent viable therapeutics to address this emerging threat. UPEC express long fibrillar appendages at their cell surface termed type 1 pili,^[6] which are tipped with FimH,^[7] to mediate attachment to superficial facet cells of the bladder epithelium. FimH is a two-domain adhesin^[8] comprised of an N-terminal lectin domain, which mediates specific recognition of mannosylated receptors on the bladder epithelium, and a C-terminal pilin domain, which anchors FimH to the tip of the pilus. Upon binding, FimH triggers host cell invasion and intracellular colonization by UPEC. A proportion of the UPEC population evades expulsion by escaping into the cytoplasm and replicating to form intracellular bacterial communities (IBCs), from which infection may propagate to neighboring cells. Formation of IBCs is part of a mechanism that allows UPEC to gain a foothold in the bladder and build up in numbers. Targeting FimH with small-molecule^[9] and multivalent carbohydrate mimetics^[10] to interfere with bacterial adhesion, invasion, and IBC and biofilm formation represents a promising therapeutic strategy for combatting recurrent and antibiotic-resistant UTIs.

In preliminary studies we identified biphenyl mannosides **2** and **3** (Figure 1) as promising antagonists of FimH by X-ray-structure-based design.^[11] Compound **3** exhibits good inhibition of FimH function using UPEC strain UTI89 as determined by a hemagglutination assay (HAI = 0.5 μ M) and biofilm assay (IC₅₀ = 1.35 μ M). This study revealed that *meta* substitution on the biphenyl B-ring with a hydrogen bond acceptor, such as the methyl amide of **3**, was optimal. Further structure-activity relationship (SAR) studies from us and others^[12] produced mannosides such as **5** and **6**, indicating that addition of a small substituent at the *ortho* position of the biphenyl A-ring leads to marked enhancements in potency. For example, *ortho*-methyl and chloro groups as with **5** and **6** were found to in-

[a] C. Jarvis, Dr. Z. Han, Prof. J. W. Janetka
Washington University School of Medicine
Department of Biochemistry and Molecular Biophysics
660 S. Euclid Ave., St. Louis, MO 63110 (USA)
E-mail: janetka@biochem.wustl.edu

[b] V. Kalas, R. Klein, J. S. Pinkner, Dr. B. Ford, J. Binkley, Dr. C. K. Cusumano,
Prof. S. J. Hultgren
Washington University School of Medicine
Department of Molecular Microbiology
660 S. Euclid Ave., St. Louis, MO 63110 (USA)
E-mail: hultgren@wusm.wustl.edu

[c] Prof. S. J. Hultgren, Prof. J. W. Janetka
Washington University School of Medicine
Center for Women's Infectious Disease Research (cWIDR)
660 S. Euclid Ave., St. Louis, MO 63110 (USA)

[d] Dr. Z. Cusumano, Dr. L. Mydock-McGrane
Fimbrion Therapeutics Inc.
4041 Forest Park Ave., St. Louis, MO 63108 (USA)

Supporting information for this article is available on the WWW under <http://dx.doi.org/10.1002/cmdc.201600006>.

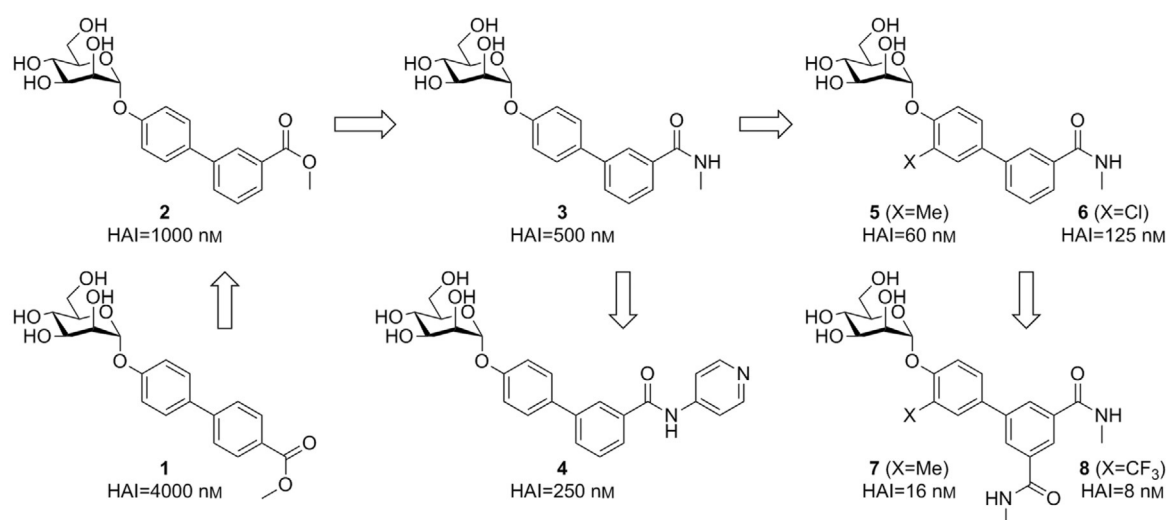


Figure 1. Progression of biphenyl α -D-mannoside FimH inhibitors.

crease HAI titers (60 and 125 nM) relative to **3** (500 nM). The addition of another B-ring substituent also improved activity (compounds **7** and **8**). This increase in potency was attributable to an increase in relative binding affinity for the FimH lectin domain as measured by differential scanning fluorimetry (DSF). In vivo investigation of mannoside **5** demonstrated that the compound is orally bioavailable and efficacious against acute,^[13] chronic,^[14] and antibiotic-resistant^[15] UTI in mice. However, despite this efficacy, the oral bioavailability of **5** is low, and compound exposure in the urine was significantly decreased by eight hours. Herein we report on newly optimized mannosides with significantly enhanced FimH potency, oral bioavailability, and efficacy in treating chronic UTIs.

To better understand the improved interactions of **5** and **7** with FimH, a high-resolution (1.67 Å) X-ray crystal structure of **7** (PDB ID: 5F2F) bound to the FimH lectin domain was obtained (Figure 2A). As noted in prior co-crystal structures,^[11a,16] the mannoside ring is bound tightly in a deep hydrophilic pocket by an intricate network of hydrogen bonds between

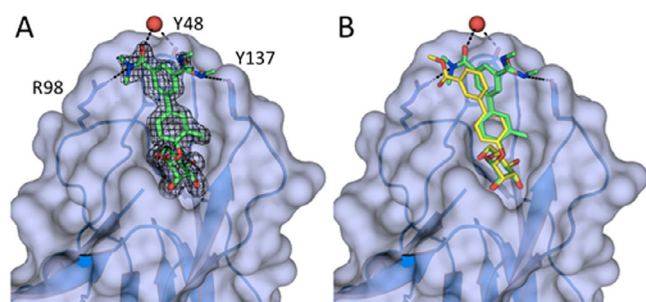


Figure 2. Structural basis of FimH-mannoside interactions. A) Crystal structure of compound **7** bound to FimH lectin domain (PDB ID: 5F2F). Unambiguous electron density from the $F_o - F_c$ map (black mesh) and contoured at 1σ reveals compound **7** (green sticks) bound in the mannoside binding pocket of FimH (blue ribbon and surface). B) Comparison of mannoside binding poses. Overlay of compound **2** (yellow sticks; PDB ID: 3MCY) on **7** bound to the FimH lectin domain.

the C2, C3, C4, and C6 hydroxy groups of mannoside and the main chain of F1 and side chains of N46, D54, Q133, N135, and D140. The O-linked aglycone projects toward the lid of the binding pocket and positions functional groups for favorable interactions. We discovered that the *ortho*-methyl substituent of the A-ring promotes hydrophobic interactions, as it packs snugly against the surface formed by I52, Y137, and N138. The B-ring phenyl forms favorable π - π stacking interactions with Y48 and the amide carbonyl of **7** indirectly interacts with the phenol of Y48 through a water-mediated hydrogen bond network, as evidenced by the ideal bent geometry and proximal distances (3–3.2 Å) of hydrogen bond donor-acceptor pairs. In addition, the secondary nitrogen atom of the two amides form electrostatic and potential H-bonding interactions with the neighboring R98 and Y137 residues, but these groups lie 4.1 and 4.6 Å away, respectively. However, the electron density of the second amide near Y137 reveals two different orientations of the amide carbonyl in which the carbonyl could be acting as an H-bond acceptor to the phenol. Comparison of mannoside **7** with **2** (Figure 2B) by structural overlay highlights a unambiguous difference in the orientation of the biphenyl group. Based on the structure of **7** presented here and a related analogue,^[12a] the improvement in activity of mannosides with *ortho*-substituted groups on the A-ring (**5**–**8**) relative to unsubstituted **2** and **3** can be explained by: 1) increased hydrophobic contact of the *ortho* substituent encompassed by the molecular surface formed by I52, Y137, and N138; 2) improved π - π stacking with Y48; and 3) decreased entropic cost of binding due to restriction in ring rotation. Altogether, this structure highlights the essential interactions that *ortho*-substituted mannosides form with the rim of the mannoside-binding pocket, or the “tyrosine gate” of Y48 and Y137, responsible for increased potency. Despite the good activity of **5** and **7** from in vitro assays, in vivo pharmacokinetic (PK) studies show that both mannosides have low oral bioavailability and half-life. We hypothesize that they are metabolically unstable from hydrolysis of the methyl amide and/or hydrolysis of the O-glycosidic

bond via the action of α -mannosidases. In an effort to improve the metabolic stability of these compounds, we examined the effects of replacing the amide with non-hydrolyzable bioisosteres.

Our structure of **7** shows an electrostatic or hydrogen bonding interaction of the *meta*-substituted amide carbonyl with R98, similar to the ester carbonyl of **2** (Figure 2B; PDB ID: 3MCY).^[11a] The importance of this interaction can be demonstrated by **1**, in which the ester is located in the *para* position, resulting in a marked decrease in potency (Figure 1). To determine whether we could mimic the amide of **3** and retain this interaction with FimH, we designed analogues with non-hydrolyzable isoelectronic and isosteric groups (Figure 3). In our earlier studies, we evaluated a small set of mannosides containing simple amide isosteres in the B-ring *meta* position, such as nitro **9**, nitrile **10**, and sulfonamide **14**. All isosteres retained similar potency, while analogues incapable of the same hydrogen bonding—phenol **11**, fluoride **12**, and methyl alcohol **13**—all lost potency relative to that of **3**. This data provided additional evidence that the salt bridge interaction with R98 provides the basis for increased FimH binding and inhibition of adhesion by the HA assay. In another set of compounds, we used nitrogen-containing heterocycles to mimic the spatial orientation and electronics of the amide carbonyl of compound **7**. Isoquinoline **15** displays similar activity as observed with **3**, while the isomeric isoquinoline analogue **17** had slightly improved activity, with $\text{HAI} = 0.25 \mu\text{M}$. This discrepancy in activity is most likely explained by the different orientations of the nitrogen, predicted to interact with R98 which mimics the carbonyl oxygen in **3**. Interestingly, the analogue with improved activity, **17**, directs the carbonyl mimic in an 'endo-like' conformation pointing in the direction of mannose, in contrast to **15**, which assumes an 'exo-like' orientation pointing away from the mannose ring. To maintain this interaction, we proposed that cyclizing or 'fusing' the amide of **3** onto the B-ring phenyl group as with isoquinolone **16** would maintain this hydrogen bonding interaction and also aid in protecting the amide from

hydrolysis. Indeed, we found that **16** shows a fivefold improvement in HA potency ($\text{HAI} = 0.1 \mu\text{M}$) over **3**. This result suggests that the isoquinolone amide carbonyl is oriented in a way that mimics the more energetically favorable binding conformation to FimH retaining the interaction with R98. This rationale can also be used to explain the increased activity of **7** over **5**. The addition of the second *meta*-substituted methyl amide in **7** proposes that the conformation where the amide is in proximity to the salt bridge (and Y48) is statistically higher than **5**.

Based on these exciting results, we synthesized new mannosides **22** and **17b**, the matched pairs of **16** and **17**, by introducing an *ortho*-methyl group on the A-ring of the biaryl aglycone to increase potency. Mannoside **22** was synthesized using two different synthetic routes, as shown in Scheme 1A and 1B. In route 1A, aryl boronate mannoside **18**^[11b] was coupled to 7-bromo-1(2*H*)-isoquinolone via a palladium-mediated cross-coupling to give protected tetraacetate **21**. In route 1B, the bromoisoquinolone was first converted into the boronate ester **19**. Suzuki cross-coupling of **19** to bromophenyl mannoside **20**^[11b] gave **21**. In both routes, mannose acetate deprotection was performed with sodium methoxide to give **22** in good yields. Isoquinoline **17b** was synthesized in a similar fashion from **18** and 5-bromoisoquinoline. When tested in the HA assay, both isoquinolone **22** and isoquinoline **17b** had a significant fourfold increase in activity (Table 1) relative to **16** and **17**, respectively.

Given the excellent potency displayed by **22**, we wanted to more closely examine its biological behavior in both in vitro and in vivo assays. We first evaluated **5**, **7**, and **22** in a biofilm prevention assay followed by a thermal shift assay by differential scanning fluorimetry (DSF) to quantitatively calculate relative binding strength to the FimH lectin domain (Table 1). Early mannosides **2** and **3** prevent biofilm formation with IC_{50} values of 0.94 and 1.35 μM , respectively, whereas **5** and **7** display ~10-fold higher potency (Table 1). We now report that **22** is equipotent to **5** and **7** in the biofilm and melting point shift assays. Upon the identification of **22**, we next turned our at-

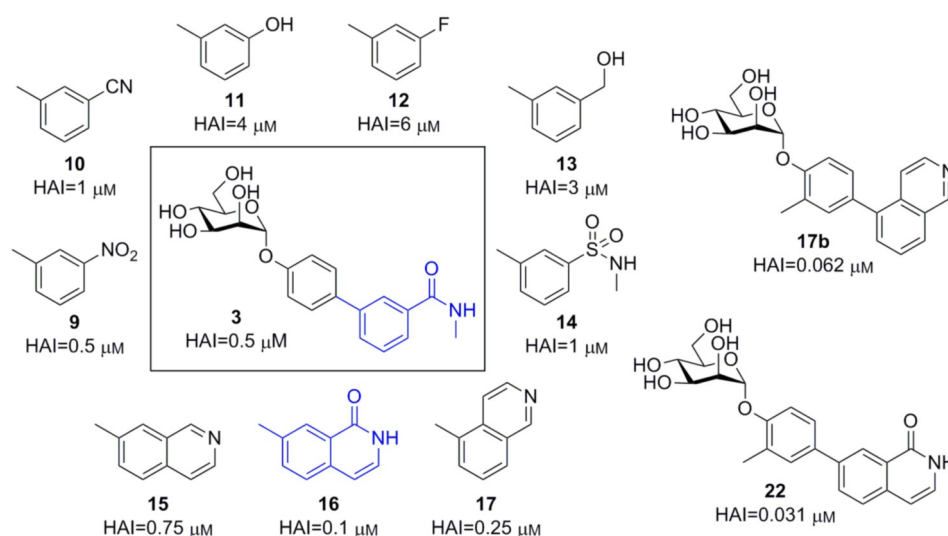
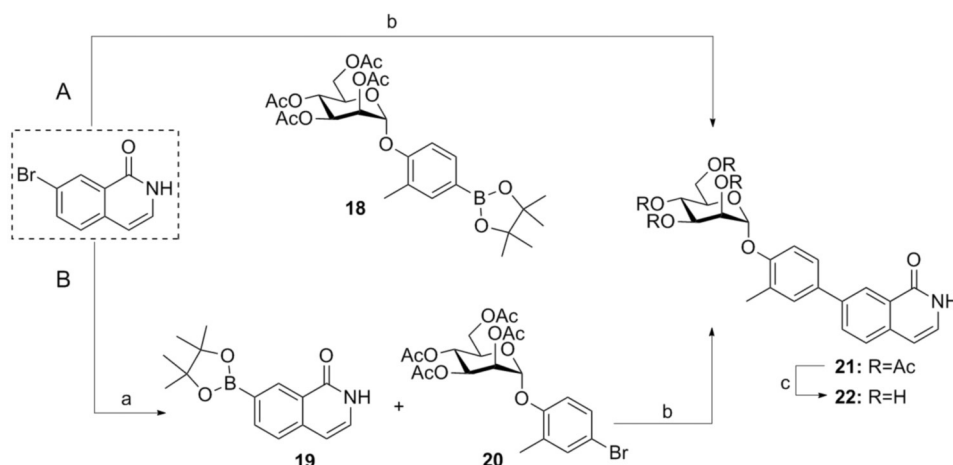


Figure 3. Potency and SAR of *meta*-position amide bioisostere analogues of biphenyl mannoside **3**.



Scheme 1. Synthesis of A-ring *o*-methyl B-ring isoquinolone mannoside **22**. Reagents and conditions: a) bis(pinacolato)diboron, cat. Pd(dppf)Cl₂, KOAc, DMSO; b) cat. Pd(PPh₃)₄, Cs₂CO₃, dioxane/H₂O, 80 °C; c) NaOMe/MeOH.

Table 1. In vitro biological and PK profile of initial and optimized mannosides.

Compd	HAI [μM]	Biofilm IC ₅₀ [μM]	DSF T _m [°C]	cLogD	Rat CL [mL min ⁻¹ kg ⁻¹] ^[a]	Rat V _{dss} [L kg ⁻¹] ^[a]	Rat F [%] ^[a]	Rat t _{1/2} [h] ^[a]
2	1.0	0.94	73.4	1.17	ND	ND	ND	ND
3	0.50	1.35	73.1	0.28	ND	ND	ND	ND
5	0.062	0.16	75.5	0.93	98	1.3	1.4	2.8
7	0.016	0.12	75.8	1.35	ND	ND	ND	ND
17b	0.062	ND	ND	1.21	ND	ND	ND	ND
22	0.031	0.13	75.5	1.4	408	6.7	7.0	<3

[a] Calculated from a 10 mg kg⁻¹ oral (p.o.) dose, 10% cyclodextrin formulation; ND: not determined.

tention to assessing the drug-like properties and pharmacokinetics of our compounds in order to prioritize them for in vivo studies. cLogD is often used as a good indicator of solubility. While mannosides are sugar-based, and are therefore predicted to have relatively good water solubility, our compounds have hydrophobic biaryl aglycones which encompass most of the molecular weight of the mannoside, causing the solubility to be variable. We calculated the LogD values of the five analogues in Table 1 and found that the change from a methyl ester **2** to amide **3** leads to a large drop in LogD from 1.17 to 0.28. Interestingly, introduction of the *ortho*-methyl group in amide **5** results in a large increase in LogD (0.93), almost recapitulating the solubility of ester **3**. More surprising is that the addition of the second methyl amide in **7** further increases the LogD to 1.35, which is identical to that of cyclic amide/quinolone **22** (LogD 1.4). Therefore, we conclude that LogD is not well correlated to the improved activity of **7** and **22**. Furthermore, evaluation in plasma and liver microsomes (Supporting Information) suggests that all compounds are metabolically stable in both mouse and human species.

Subsequently, we performed an in vivo pharmacokinetic (PK) study of the three lead mannosides in mice. In past studies, we have correlated compound levels in the urine at 6 h post-dosing as a good predictor of pharmacodynamic (PD) efficacy. Therefore, compounds were dosed via oral gavage (formulated in 10% cyclodextrin) at 50 mg kg⁻¹. Urine was collected at sev-

eral time points (1, 3, and 6 h), and mannoside concentration was determined by mass spectrometry. As illustrated in Figure 4A, the initial urine concentration of **7** and **22** were elevated relative to **5** at 1 h post-dosing, but level off and then display lower clearance for the remainder of the time course. A follow-up i.v./p.o. crossover study of **5** and **22** in rat (Table 1; Supporting Information), revealed that **22** (p.o. dose at 10 mg kg⁻¹) has higher bioavailability ($F=7.0\%$) than **5**, but also higher clearance ($CL=408$) and a larger volume of distribution ($V_{dss}=6.7$ L kg⁻¹). Finally, we tested the lead mannosides in a murine model of chronic UTI, which was described previously.^[14] Briefly, introduction of bacteria into the urinary tract results in an acute infection, which in a subpopulation of mice can progress to a chronic infection as a result of an over-exuberant host response. Chronic infection is defined by severe pyuria and persistent bacteriuria. Elimination of bacteria in mice with chronic UTI requires antibiotic treatment. Shown in Figure 4B, all three compounds showed excellent efficacy relative to the control group, significantly dropping the bacterial burden (CFUs per bladder) of chronically infected mice by several log units. Excitingly, lead **22** displayed the best efficacy with a substantial 10-fold additional drop in CFUs per bladder relative to **5**, **7**, and isoquinoline analogue **17b** (Supporting Information). The enhanced efficacy over **5** and **7** can be rationalized from the increased bioavailability of **22** and possibly the high volume of distribution (V_{dss}), indicating substantial tissue

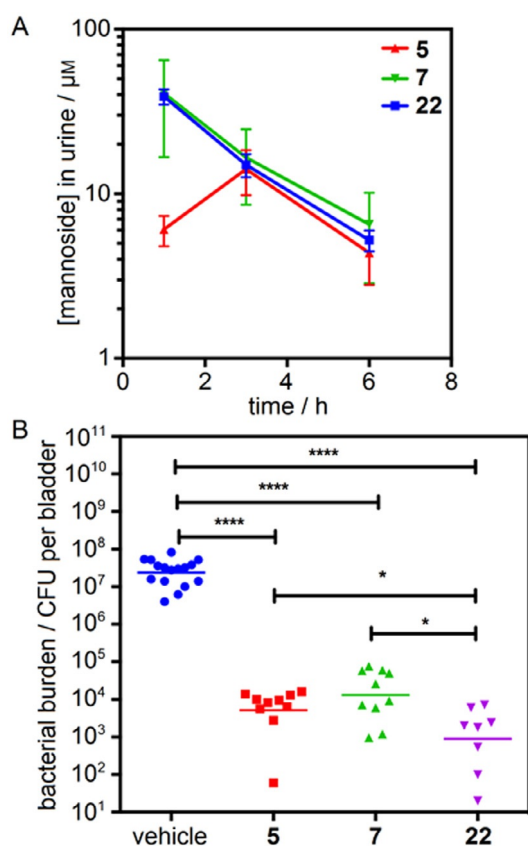


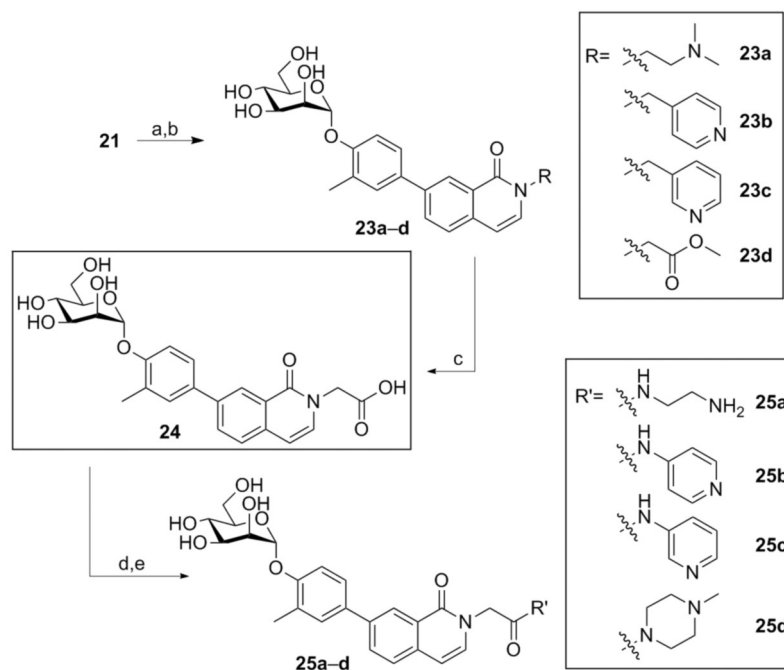
Figure 4. Mannoside PK/PD. A) In vivo mouse PK of **5**, **7**, and **22** following oral delivery at 50 mg kg^{-1} . Urine mannoside concentrations over time indicate equivalent concentrations of **7** and **22**. Data are the mean \pm SEM from at least three animals. B) In vivo mouse PD model of UTI89 chronically infected mice dosed with **5**, **7**, and **22** at 50 mg kg^{-1} p.o. (10% cyclodextrin formulation). Compound **22** shows significantly 10-fold enhanced efficacy relative to **5** and **7** at 6 h post-dosing. Differences were tested for significance within the designated treatments using Mann–Whitney U-test (**** $p < 0.0001$, * $p < 0.05$).

exposure, which is also supported by its rapid clearance (CL). The new lead mannoside **22** has elevated potency, better drug-like physical properties, bioavailability, and improved in vivo efficacy. To further improve the drug oral bioavailability and half-life, we synthesized a series of N-substituted mannosides based on **22**, designed to explore structure–property relationships (SPR), specifically the effects of pK_a on half-life, clearance, tissue exposure, and oral bioavailability.

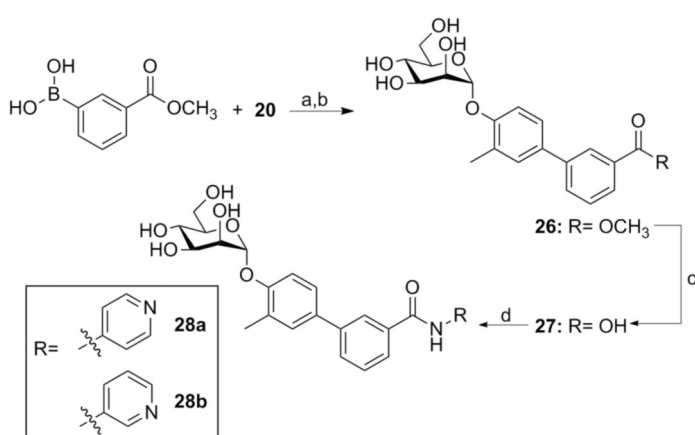
To access this library based on **22**, we used a synthetically feasible route for regioselectively substituting the isoquinolone nitrogen versus the oxygen. Thus, substitution reactions with isoquinolone **21** were performed with various alkyl bromides as shown in Scheme 2. Subsequent acetyl deprotection with NaOMe/MeOH was completed to obtain target mannosides **23 a–d** in respectable yields. Acetamide ester **23 d** was used as a key intermediate to access further diversity in substitution of the isoquinolone through installation of a terminal amide. To this end, saponification of **23 d** to carboxylic acid **24**, followed by standard peptide coupling to various amines with HATU, produced isoquinolone mannosides **25 a–d** in excellent yields. These compounds were designed to combine the conforma-

tional restrictions of the isoquinolone ring and the increased basicity of the ester- and amine-bearing substituents, in an attempt to improve both affinity and PK. To verify that the rigidity afforded by the isoquinolone moiety in compounds **23–25** was responsible for the increase in binding observed, we synthesized compounds **28 a–b** to maintain similar interactions, while affording greater flexibility in the FimH binding pocket. We used a similar route involving a Suzuki cross-coupling of 4-methoxycarbonylphenylboronic acid to bromophenyl mannoside **20**, followed by saponification of compound **26** to **27**, and subsequent HATU-mediated amine coupling (Scheme 3). Subsequent to synthesis, the focused set of substituted quinolones were tested in the HA, biofilm, and DSF assays described above. Shown in Figure 5, almost all analogues of **22** had improved activity in the HA and biofilm assays at a level correlating well with the relative increased binding strength by DSF. The pyridyl acetamides **25 b** and **25 c** were identified as the most potent analogues, with nearly identical activity ($\text{HAI} = 1 \text{ nM}$, biofilm $\text{IC}_{50} = 20 \text{ nM}$, and DSF $T_m = 76.3^\circ\text{C}$). While the two acyclic amide derivatives, **28 a** and **28 b**, display potency (31 and 62 nM) in the HA assay, their matched quinolone pairs, **23 b** and **23 c**, have better HAI titers of 4 and 8 nM. As elucidated by DSF melting point data, this notable eightfold enhancement in activity is derived largely from increased FimH binding as a result of the conformational restriction of the amide in quinolones **23 b** and **23 c**. Notably, the intermediate acid **24**, used to synthesize **25 b** and **25 c**, showed a lower DSF melting temperature ($T_m = 74.8^\circ\text{C}$) and biofilm inhibition with an IC_{50} value of 120 nM, whereas the HA inhibition assay showed an improvement, with $\text{HAI} = 16 \text{ nM}$. Interestingly, when evaluated for oral PK in rats (Supporting Information), we discovered that the two analogues **23 b** and **25 d** showed only minor evidence of bioavailability and when tested in the animal model of chronic UTI, analogues **23 a** and **23 c** showed no significant effect in decreasing the bacterial burden in mice when dosed orally (50 mg kg^{-1}). On the other hand, **28 b** displayed similar activity to that of **5** and **7** in the animal model (Supporting Information). The basis for the lack of oral bioavailability or efficacy in mice or rats remains unclear. All substituents of **22** have a basic, high pK_a and create a tertiary amide on the mannoside, so it is possible that either change prompts alternate metabolism in the stomach, gut, and/or plasma, resulting in the lack of oral exposure. Nonetheless, this new class of quinolone mannosides has the highest FimH affinity and potency of any antagonists reported to date (e.g., **25 b** $\text{HAI} = 1 \text{ nM}$). They are also capable of preventing bacterial biofilm formation of UPEC at activity levels well below that of any previously reported small molecule (e.g., **25 c** biofilm $\text{IC}_{50} = 18 \text{ nM}$).

The development of small-molecule antagonists of the type 1 pilus adhesin FimH for the clinical treatment and prevention of UTI holds promise as an antibiotic-sparing strategy. Our current pursuit in identifying a compound for clinical development has involved a number of lead optimization studies on improving interactions with FimH, as well as understanding structure–property relationships from these modifications in vivo. In this study we pursued a structure-based approach in which we obtained a high-resolution X-ray structure of **7**



Scheme 2. Synthesis of isoquinolone mannoside analogues with varied pK_s substituents. *Reagents and conditions:* a) Br-R, NaH, DMF, 0 °C; b) NaOMe/MeOH (0.02 M), RT; c) NaOH (0.2 M), MeOH, RT; d) HATU and DMF added at 0 °C, DIEA and 1°/2°-amine-R' added, brought to RT; e) NaOMe/MeOH (0.02 M), RT.



Scheme 3. Synthesis of acyclic mannoside amides as matched pairs to pyridyl isoquinolones **23b–c** and **25b–c**. *Reagents and conditions:* a) cat. Pd(PPh₃)₄, Cs₂CO₃, dioxane/H₂O, 80 °C; b) NaOMe/MeOH (0.02 M), RT; c) NaOH (0.2 M), MeOH, RT; d) HATU and DMF added at 0 °C, DIEA and 1°-amine added and brought to RT.

bound to FimH for identifying key interactions aimed at improved potency. Mannosides containing simple isosteric or isoelectronic replacements of the biaryl B-ring amide^[11–12] have been previously studied and have similar potency and properties to those having the amide. In contrast, the conformationally restricted cyclic amide isoquinolone and isoquinoline isosteres reported herein produce improved mannosides with significantly elevated potency, better drug-like properties, and in vivo efficacy. Consequently, quinolone mannoside **22** has substantially improved bioavailability and a 10-fold increased efficacy in the treatment of chronic UTI in mice. Furthermore, substitution of **22** has led to a new class of the most potent

isoquinolone-based mannosides ever reported. In summary, we have discovered new lead biaryl mannoside **22**, which is a promising preclinical candidate drug for the treatment and prevention of urinary tract infections.

Abbreviations: UTI, urinary tract infection; UPEC, uropathogenic *E. coli*; SAR, structure–activity relationship; HA, hemagglutination; HAI, HA inhibition titer; IBCs, intracellular bacterial communities; PD, pharmacodynamics; PK, pharmacokinetics.

All animal studies using mice were approved by the Animal Studies Committee of Washington University (Animal Protocol Number 20150226).

Acknowledgements

We thank Jan Crowley and Jeff Henderson (NIH MS facility, cWIDR) for generating bioanalytical data from the PK studies, Rick Stegeman (X-ray facility, Biochemistry Department) for help with X-ray crystallography, and Scott Wildman (Biochemistry Department) for help with molecular modeling and docking of FimH ligands. This project was funded in part by US National Institutes of Health (NIH) grants 1RC1K086378 (Washington University) from the National Institute of Diabetes and Digestive and Kidney Diseases (NIDDK), and 1R43AI106112-01A1 (Fimbrion Therapeutics, Inc.) from the National Institute of Allergy and Infectious Diseases (NIAID).

Keywords: biofilms · FimH · mannosides · urinary tract infections · uropathogenic *E. coli*

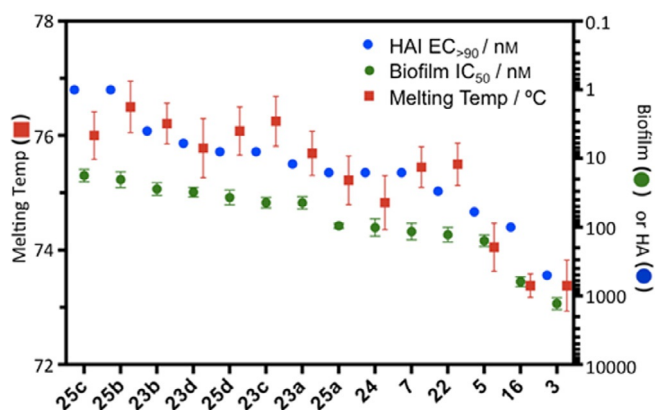


Figure 5. Summary plot of mannoside structure–activity data as measured by hemagglutination inhibition (HAI) assay (EC_{90}), biofilm prevention assay (IC_{50}), and DSF thermal shift assays (T_m). Good correlation of mannoside activity in the HAI and biofilm prevention assays are observed when plotted against the relative binding strengths derived from the DSF melting point assay.

- [1] A. L. Flores-Mireles, J. N. Walker, M. Caparon, S. J. Hultgren, *Nat. Rev. Microbiol.* **2015**, *13*, 269–284.
- [2] a) M. G. Blango, M. A. Mulvey, *Antimicrob. Agents Chemother.* **2010**, *54*, 1855–1863; b) M. Totsika, S. A. Beatson, S. Sarkar, M. D. Phan, N. K. Petty, N. Bachmann, M. Szubert, H. E. Sidjabat, D. L. Paterson, M. Upton, M. A. Schembri, *PLoS One* **2011**, *6*, e26578.
- [3] a) T. J. Hannan, I. U. Mysorekar, C. S. Hung, M. L. Isaacson-Schmid, S. J. Hultgren, *PLoS Pathog.* **2010**, *6*, e1001042; b) I. U. Mysorekar, S. J. Hultgren, *Proc. Natl. Acad. Sci. USA* **2006**, *103*, 14170–14175.
- [4] B. Foxman, *Dis.-Mon.* **2003**, *49*, 53–70.
- [5] D. A. Rasko, V. Sperandio, *Nat. Rev. Drug Discovery* **2010**, *9*, 117–128.
- [6] S. D. Knight, J. Bouckaert, *Top. Curr. Chem.* **2009**, *288*, 67–107.
- [7] S. Geibel, E. Procko, S. J. Hultgren, D. Baker, G. Waksman, *Nature* **2013**, *496*, 243–246.
- [8] a) M. A. Schembri, K. Kjaergaard, E. V. Sokurenko, P. Klemm, *J. Infect. Dis.* **2001**, *183*, S28–S31; b) D. Choudhury, A. Thompson, V. Stojanoff, S. Lan-

germann, J. Pinkner, S. J. Hultgren, S. D. Knight, *Science* **1999**, *285*, 1061–1066.

- [9] a) J. Bouckaert, J. Berglund, M. Schembri, E. De Genst, L. Cools, M. Wuhler, C. S. Hung, J. Pinkner, R. Slattegard, A. Zavialov, D. Choudhury, S. Langermann, S. J. Hultgren, L. Wyns, P. Klemm, S. Oscarson, S. D. Knight, H. De Greve, *Mol. Microbiol.* **2005**, *55*, 441–455; b) N. Firon, S. Ashkenazi, D. Mirelman, I. Ofek, N. Sharon, *Infect. Immun.* **1987**, *55*, 472–476; c) L. K. Mydock-McGrane, Z. T. Cusumano, J. W. Janetka, *Expert Opin. Ther. Pat.* **2016**, in press; DOI: 10.1517/13543776.2016.1131266.
- [10] M. Hartmann, T. K. Lindhorst, *Eur. J. Org. Chem.* **2011**, 3583–3609.
- [11] a) Z. F. Han, J. S. Pinkner, B. Ford, R. Obermann, W. Nolan, S. A. Wildman, D. Hobbs, T. Ellenberger, C. K. Cusumano, S. J. Hultgren, J. W. Janetka, *J. Med. Chem.* **2010**, *53*, 4779–4792; b) Z. Han, J. S. Pinkner, B. Ford, E. Chorell, J. M. Crowley, C. K. Cusumano, S. Campbell, J. P. Henderson, S. J. Hultgren, J. W. Janetka, *J. Med. Chem.* **2012**, *55*, 3945–3959.
- [12] a) S. Kleeb, L. Pang, K. Mayer, D. Eris, A. Sigl, R. C. Preston, P. Zihlmann, T. Sharpe, R. P. Jakob, D. Abgottspon, A. S. Hutter, M. Scharenberg, X. Jiang, G. Navarra, S. Rabbani, M. Smiesko, N. Ludin, J. Bezencon, O. Schwardt, T. Maier, B. Ernst, *J. Med. Chem.* **2015**, *58*, 2221–2239; b) L. J. Pang, S. Kleeb, K. Lemme, S. Rabbani, M. Scharenberg, A. Zalewski, F. Schadler, O. Schwardt, B. Ernst, *ChemMedChem* **2012**, *7*, 1404–1422; c) O. Schwardt, S. Rabbani, M. Hartmann, D. Abgottspon, M. Wittwer, S. Kleeb, A. Zalewski, M. Smiesko, B. Cutting, B. Ernst, *Bioorg. Med. Chem.* **2011**, *19*, 6454–6473; d) T. Klein, D. Abgottspon, M. Wittwer, S. Rabbani, J. Herold, X. H. Jiang, S. Kleeb, C. Luthi, M. Scharenberg, J. Bezencon, E. Gubler, L. J. Pang, M. Smiesko, B. Cutting, O. Schwardt, B. Ernst, *J. Med. Chem.* **2010**, *53*, 8627–8641.
- [13] P. S. Guiton, C. K. Cusumano, K. A. Kline, K. W. Dodson, Z. F. Han, J. W. Janetka, J. P. Henderson, M. G. Caparon, S. J. Hultgren, *Antimicrob. Agents Chemother.* **2012**, *56*, 4738–4745.
- [14] C. K. Cusumano, J. S. Pinkner, Z. Han, S. E. Greene, B. A. Ford, J. R. Crowley, J. P. Henderson, J. W. Janetka, S. J. Hultgren, *Sci. Transl. Med.* **2011**, *3*, 109ra115.
- [15] M. Totsika, M. Kostakioti, T. J. Hannan, M. Upton, S. A. Beatson, J. W. Janetka, S. J. Hultgren, M. A. Schembri, *J. Infect. Dis.* **2013**, *208*, 921–928.
- [16] B. Fiege, S. Rabbani, R. C. Preston, R. P. Jakob, P. Zihlmann, O. Schwardt, X. Jiang, T. Maier, B. Ernst, *ChemBioChem* **2015**, *16*, 1235–1246.

Received: January 5, 2016

Published online on January 26, 2016